# A fast efficient multi-scale approach to modelling the development of hydride microstructures in zirconium alloys

Mitesh Patel[1], Luca Reali[1], Adrian P. Sutton[1], Daniel S. Balint[2], and Mark R. Wenman[3]

[1]*Department of Physics, Imperial College London, UK*
[2]*Department of Mechanical Engineering, Imperial College London, UK*
[3]*Department of Materials and Centre for Nuclear Engineering, Imperial College London, UK*

**Abstract**

A mechanistic understanding of hydrogen diffusion and hydride precipitation at the microscale underpins the prediction of delayed hydride cracking in zirconium alloy nuclear fuel cladding. We present a novel approach to modelling the microstructures created by hydride precipitation at loaded notches in polycrystalline Zr alloys. The model is multi-scale in that it includes the elastic dipole tensor of interstitial hydrogen in α-Zr, it treats the stress-driven diffusion of hydrogen at the meso-level (mm), it calculates the thermodynamically favourable spatial arrangement of microhydrides and their assembly into macrohydride colonies, in a textured polycrystalline sample, and it treats the full elastic field of the loaded notch and all the hydrides at a scale similar to the cladding thickness. A simplifying innovation is the representation of the elastic field of a microhydride by a dislocation dipole, where the Burgers vector is set to create the experimentally measured strain in the $\langle 1\bar{1}00\rangle$ direction. The model provides a predictive framework for treating elastic anisotropy, a variety of potential nucleation sites, and different grain sizes. Simulated micrographs of hydride networks in polycrystalline samples with blunt and sharper loaded notches are compared with experimental micrographs obtained at the same scale. The simulations are extremely fast and calculations typically take around tens of seconds. This makes it possible to carry out detailed sensitivity studies with respect to several pertinent metallurgical variables, as well as conducting ensemble averaging of hydride microstructures.

**Keywords**— Hydride precipitation and reorientation, Multi-scale modelling, Zirconium

## 1 Introduction

Zirconium alloys are used in water-cooled fission reactors both for fuel cladding and as structural material. Zirconium combines good mechanical properties, corrosion resistance and a very low thermal neutron absorption cross-section [1]. The use of water as coolant requires that the alloys resist the detrimental effect of hydrogen, which leads to the precipitation of hydrides. This causes an embrittlement that reduces the life of the nuclear fuel and is the origin of delayed hydride cracking (DHC). DHC is a specific time-dependent failure process characterised by H accumulating at stress concentrators and then precipitating as hydrides. If the notch-tip hydride breaks, the newly formed crack attracts more H, leading to more hydrides precipitating, and the process can start anew [2]. In service, the dissociation of the coolant water produces the zirconium oxide film while a fraction of the hydrogen produced enters the metal [3]. Hydrogen has a low solubility limit in Zr-alloys, negligible at room temperature and increasing to ∼400 wppm at 500 °C [2]. During service the total H concentration continually increases, and at some point reaches 100s of wppm, meaning that there are hydrides in the microstructure. Furthermore, the number of hydrides increases significantly during the reactor shut-down cycles.

To develop a physically based model for hydride precipitation, it is necessary to start from the hydride crystallography and morphology. We note that the hydrides are studied both at the macroscopic optical microscope scale and at the nano-microscopic transmission electron microscope (TEM) scale. At the former scale, they appear as single, compact objects that we refer to as macrohydrides and they may be up to many 100s of microns in length. In the TEM it is seen that the macrohydrides are made of a stack of smaller individual microhydrides (Fig 2a) with a typical length of 100s of nm to a few microns [4].

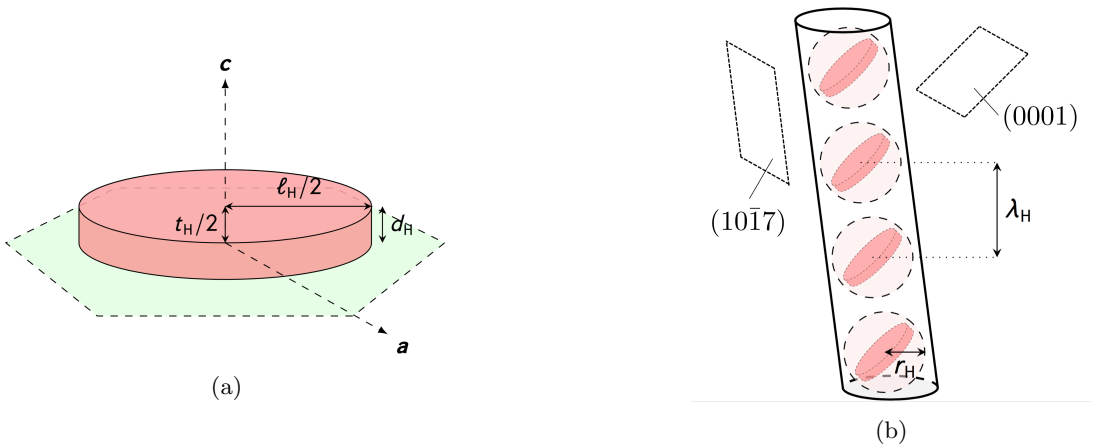


Figure 1: (a) The microhydride is approximated as an elliptical disc lying on the basal plane, whose major semi-axis is aligned along one of the three $\langle 11\bar{2}0\rangle$ directions. A segment of the three dimensional stacking of the microhydrides in a macrohydride with the simplest observed substructure is schematically depicted in (b). The microhydrides have a spacing $\lambda_H$ and lie on multiple basal planes, while the macrohydride lies on a near-basal $(10\bar{1}7)$ plane. The angle (14.7°) between (0001) and $(10\bar{1}7)$ planes is enlarged for clarity.

Four hydride phases have been reported to date. In order of increasing H content they are classified according to their stoichiometry as the hexagonal (hcp) ζ-$ZrH_{0.5}$, face-centred tetragonal (fct) γ-ZrH, face-centred cubic (fcc) δ-$Zr_2H_3$ and fct ε-$ZrH_2$. The latter three, however, may also be thought of as a common Zr lattice with a face-centred symmetry where H occupies an increasing number of tetrahedral interstices and changes the $c/a$ ratio from >1 (γ) to 1 (δ) to <1 (ε). If the γ phase is stoichiometric [2], the δ phase can have an atomic ratio H/Zr in the range 1.4-1.7, above which the transition to the ε phase begins [5]. The two phases of interest in the nuclear industry are primarily the γ and δ deemed to be responsible for the mechanical degradation of Zr-alloys [3].

The microhydrides are found to satisfy a specific orientation relationship with the parent phase. The minimisation of the energy upon precipitation ensures that the close-packed planes and directions are aligned [6, 7, 8], i.e.

$$\{0001\}_\alpha \parallel \{111\}_{\gamma/\delta}$$
$$\langle 11\bar{2}0\rangle_\alpha \parallel \langle 1\bar{1}0\rangle_{\gamma/\delta}.$$

The hydrides precipitate on different habit planes, the basal {0001} being the most common [2]. The direction of growth is the $\langle 11\bar{2}0\rangle$ [3].

All the hydride phases are less dense than zirconium, and there is an anisotropic transformation strain to be accommodated. In the model, we adopt the transformation strain tensor for the microhydrides that has been calculated for the γ hydrides by Carpenter and co-workers [4]. The strain in the $\langle 11\bar{2}0\rangle$ direction has a very low value of 0.6 %, whereas the mismatch in the $\langle 1\bar{1}00\rangle$ direction is 5.6 %. This was used to explain their needle-like morphology.

In this work we assume the microhydrides are needles parallel to the basal plane. We assume the dominant misfit is normal to the habit plane of these needles. The needle morphology is approximated as an elliptical disc, as illustrated in Fig. 1a, where all the misfit is confined to the circumference of the disc and is along the c-axis. By varying the ratio between the semi-axes $l_H/2$ and $t_H/2$ of the elliptical faces both thin needles and platelets can be modelled. The macrohydrides also have a habit plane, which is generally reported to be approximately $(10\bar{1}7)$. The microhydrides precipitate in the deck-of-cards fashion of Fig. 1b, as sketched in Fig. 13 in [9], observed experimentally in Fig. 13 in [10] and modelled in Fig. 15 in [11]. This was observed both for the γ [6] and for the δ hydride, irradiated [9] or unirradiated [10, 12].

It is well known that the hydride precipitation is strongly affected by stress. In particular, the hydrides tend to orient normal to the applied stress [13]. This is at the origin of the characteristic patterns found at the notch tips (see e.g. Fig. 5 in [14]). It is also confirmed by the fact that if in unstressed tubes the hydrides precipitate in the circumferential direction, when a bending stress is applied above a certain threshold they start following the hoop stress and precipitate in the radial direction [15].

Radial hydrides, whether at the inner rim of the cladding or at the root of a notch, have a much more detrimental effect on the ductility of the Zr-alloys [9, 13]. Therefore, being able to model the hydride precipitation, taking

explicit account of the microstructure, is a first step towards a new approach in modelling hydride reorientation, and possibly DHC. The aim is predicting DHC initiation and/or failure as a function of the notch geometry, alloy microstructure and thermomechanical cycling. However, the flourishing literature on this topic shows that the matter is still far from being fully understood. The complexity of DHC stems from the considerable transformation strains involved with the hydride precipitation [2], and taking them into consideration is a key ingredient of our modelling strategy. We also take into account explicitly two consequences of hydride precipitation in the stress field of a loaded crack or notch. First, the accommodation stresses associated with hydrides alter the elastic field of the crack, affecting subsequent diffusion of hydrogen towards the crack. Second, the precipitation of hydrides depletes the local hydrogen concentration field, which also affects further precipitation.

*It is important to put the different modelling techniques that have been used to tackle the problem of DHC in the context of their typical length scales, bearing in mind that the cross-section of the cladding, and the notch features of interest for DHC in industry, are in the mm range. Techniques used thus far are density functional theory (DFT), molecular dynamics (MD), phase field modelling (PFM) and the finite element method (FEM). Notable studies involving these techniques will be briefly reviewed in what follows. As far as their typical length scales are concerned, with DFT one can model up to a few thousands of atoms [16]. MD, on the other hand, is limited to the sub-micron scale (e.g. ∼20 nm for the side of the simulation cell in [17]). PFM can reach the microstructural scale, but cannot go beyond a few µm, even in its 2D formulation. Computational models of DHC and of the hydride phases have been reviewed by Bair et al. [3].* So far, only FEM reaches the length scale of millimetres, characteristic of DHC, and is therefore widely used in industrial practice. The purpose of these FEM models is to derive DHC parameters such as a crack opening velocity, but they are not concerned with the explicit development of the hydrided microstructure. The other aforementioned techniques, albeit unable to reach the length scale of DHC, proved useful for either a mechanistic understanding or for informing larger-scale models.

At the atomic scale, inelastic neutron scattering shows that at 600 °C the hydrogen occupies the tetrahedral site, with very few H atoms in octahedral sites [18]. DFT has since been used to confirm preference for tetrahedral occupancy [19, 20, 21, 22], even taking into account the zero point energy. DFT can be used to study properties of bulk zirconium hydrides such as their lattice constants and elastic properties [5, 23] and to assess the embrittling effect of H on Zr, by calculating the surface energy and the unstable stacking fault energy for the pure zirconium phase, the Zr-H solid solution and the pure hydride phase [24]. The elastic dipole tensor, which describes the stress caused by the presence of H in the Zr lattice, was measured by MacEwen et al. [25]. Subsequently, Nazarov et al. [26] used DFT to calculate the dipole tensor for H occupying a tetrahedral interstitial site in zirconium, which was in qualitative agreement with the measured values. Here, we use the DFT values. It should be emphasised that using the dipole tensor is the only way to account for the anisotropy of the Zr-H system and the polycrystalline heterogeneity composed on individual hcp crystallites.

On a slightly larger scale, but still of fractions of a micron, one may want to use MD. However, not many MD studies can be found due to the poor reliability and transferability of the interatomic potentials [3]. Nonetheless, Zhang et al. [17] provided some insight into the homogeneous hydride nucleation by showing that the transformation path $\alpha$-Zr$\rightarrow\zeta\rightarrow\gamma$ is possible at the reactor temperature. Their simulations show a higher stability of the fcc structure at a H/Zr atomic ratio higher than 0.5. Although they clarify that the potential they use overestimates the stability of the solid solution, this suggests that the local H concentration should locally reach very high levels before precipitation, as they too state.

PFM is widely used to simulate the growth of microhydrides. To do so, PFM combines elements of atomistics with continuum elasticity and diffusion models. References to a number of such studies can be found in Ref. [3]. PFM is able to describe the evolution in space and time of a microstructure using a set of conserved and non-conserved variables [27]. It can incorporate the effects of uniform and non-uniform stress fields, as well as the anisotropy of the transformation strain. Published larger scale DHC models cannot retain the exact details of the hydride morphology and precipitation. According to Shi and Xiao [27] such details would have a strong effect on the fracture behaviour. When first applied to the study of hydrides [28, 29], PFM was scale-invariant and therefore only used to understand different hydride morphologies phenomenologically [3]. This means that the same model could be applied to micro or macrohydrides, depending on the dimensions to which the results were compared. Shi and Xiao developed a quantitative version of the model, able to compare directly with TEM images and to predict length, shape and orientation of the $\gamma$ hydrides [27], and to study the temperature-dependent $\delta$ hydride formation [30]. The works so far presented, like others reviewed in [3], were performed under the single-crystal approximation. One example on polycrystalline zirconium is from Bair et al., who simulated 9 grains in a 6 µm × 6 µm cell under isothermal conditions, with a simulation time of ∼1 week on a computer with 20 CPU cores and 128 GB RAM capacity [31]. Another example is by Heo and colleagues, who developed a 3D model with 13 grains [32] to investigate the effect of both different levels of interfacial coherency and of the grain boundaries. However, this

required to limit the size of the simulated grains to around 50 nm in diameter. Work by Han et al. [11] used PFM to correctly predict the stack of δ microhydrides on the basal plane that results in a macrohydride feature having an apparent $(10\bar{1}7)$ habit plane, as experimentally shown by Perovic et al. [10] about 35 years before. Their study is three-dimensional, but involves a single macrohydride in a single crystal. None of the quantitative PFMs to date have surpassed the length scale of a few micrometres, thus reaching that required to simulate the full microstructure that is typical of DHC.

To develop a model that treats explicitly the evolution of the full microstructure of interest for DHC, a completely new approach is proposed. The aim is to be able to reach the length scale of hydrided microstructures with respect to a defect such as a notch of several hundred microns, while retaining the full crystallographic description of hydride precipitation that so far only PFM has reached. DHC models currently assess the likelihood of DHC initiation according to the enhancement of the hydrogen concentration at the notch-tip, which is a very conservative approach. One should also take into consideration other factors such as texture, grain size, availability of heterogeneous nucleation sites and irradiation defects, which may have a strong influence on hydride precipitation. Notch geometries that lead to a similar H concentration profile may lead to different hydride network configurations. Predicting the effects of all these microstructural factors on hydride precipitation has been the goal of our work. DFT, PFM and FEM can always be used for one-off calculations. Our model, though, should be used for capturing the underlying mesoscale complexity, exploring the parameter space with computational efficiency, statistical averaging over ensembles of simulated micrographs. Moreover, it does so with a visual, intuitive output to help the design engineers at the development stage in industry.

# 2 Outline of the model

Hydride precipitation and reorientation involves hydrogen diffusing in a stress field. Hydrides precipitate where the concentration of hydrogen is sufficiently high and nucleation is favourable. The orientation of the hydrides is not random, but is influenced by the stress (for the macrohydrides) and by the texture, the presence of other hydrides and sites where the energy for nucleation is lowered (for the microhydrides). In this section, four key ingredients of the model, necessary to explain these features, are outlined.

The first is the elastic interaction energy between the local elastic strain field and a hydrogen atom. For this we use the dipole tensor obtained by DFT [26] for a hydrogen atom occupying a tetrahedral interstitial site in Zr. The use of the dipole tensor enables the axial symmetry of the tetrahedral interstitial site to be captured fully in the elastic interaction energy. It provides a more accurate description of the elastic interaction energy than the usual misfitting sphere model, e.g. [33], of the interstitial defect where it interacts with the local hydrostatic pressure. The second is the simplification of the elastic field of a microhydride as an edge dislocation dipole. The third is a theory of diffusion-controlled precipitation, which assumes heterogeneous nucleation at high-energy sites (i.e., sites at which the nucleation energy barrier is reduced) when the local concentration exceeds a certain threshold. Fourth, we have derived the elastic fields of slit cracks and notches of various geometries analytically or semi-analytically in isotropic and anisotropic elasticity. We will use the circular-shaped notch in this work. We evaluate the total elastic field arising from cracks, notches and microhydrides represented as dislocation dipoles, as a linear superposition of these analytic expressions. Although these expressions are very algebraically long, especially in anisotropic elasticity, their analytic nature enables them to be computed extremely rapidly. Tab. 1 summarises the parameters used in our model. *Some values were taken from existing literature, some were calibrated so as the results of the model would match experimental microstructures. We carried out an initial sensitivity analysis e.g. varying $r^{(\alpha)}$ and $l_H$ by a factor of 5, finding that the optimal value should be within the given range. A full exploration of the parameter space is beyond the scope of this concept paper, but will be an important step of the implementation of this model concept into an industrial code.*

## 2.1 The separation of diffusion and precipitation

Hydrogen diffuses to regions where its chemical potential is lower in the zirconium matrix. Its chemical potential is defined as

$$\mu_H(\mathbf{x}) = \mu_H^0 + k_B T \ln\left[a_H c(\mathbf{x})\right] + E_{int}(\mathbf{x}), \tag{1}$$

where $k_B$ is Boltzmann's constant and $a_H$ is the activity coefficient of hydrogen in zirconium. We assume $a_H$ is constant. $\mu_H^0$ is a constant reference chemical potential. The hydrogen concentration $c$ and the elastic interaction energy $E_{int}$ depends on position $\mathbf{x}$. In this work we calculate the elastic interaction energy as follows:

$$E_{int}(\mathbf{x}) = -\rho_{ij}\varepsilon_{ij}(\mathbf{x}), \tag{2}$$

Table 1: Parameters of the model: material properties, microstructural features, hydrogen diffusion and precipitation. References are included when appropriate.

| | Parameter | Symbol | Value |
|---|---|---|---|
| Material properties | Elastic constants [34] | $S_{11}$ | 10.20 $TPa^{-1}$ |
| | | $S_{12}$ | -4.09 $TPa^{-1}$ |
| | | $S_{13}$ | -2.46 $TPa^{-1}$ |
| | | $S_{33}$ | 8.01 $TPa^{-1}$ |
| | Lattice constants [5] | $a$ | 3.23 Å |
| | | $c$ | 5.15 Å |
| Microstructure | Average grain size | $\langle l_g \rangle$ | 50 µm |
| | Nucleation sites density | $\rho^{(\alpha)}$ | 1/grain |
| | Average nucleation site radius | $r^{(\alpha)}$ | 5-25 µm |
| Hydrogen diffusion | Dipole tensor [26] | $\rho_{11} = \rho_{22}$ | 1.68 eV |
| | | $\rho_{33}$ | 1.74 eV |
| | Initial matrix H concentration | $c_0$ | 100 ppm |
| | Solvus | $c_{solvus}$ | $7.50c_0$ |
| Hydrogen precipitation | Misfit in the basal plane [4] | $\varepsilon_{\langle 11\bar{2}0 \rangle}$ | 0.55 % |
| | | $\varepsilon_{\langle 1\bar{1}00 \rangle}$ | 5.64 % |
| | microhydride length | $l_H$ | 1-5 µm |
| | Stack separation | $\lambda$ | $l_H/4$ |

where $\rho_{ij}$ is the dipole tensor for hydrogen occupying a tetrahedral interstitial site in Zr and $\varepsilon_{ij}$ is the elastic strain tensor of all the other defects present at the site of the hydrogen atom. Summation is implied from 1 to 3 whenever there are repeated subscripts. The elastic interaction energy is responsible for driving hydrogen to tensile regions.

The anisotropy of the elastic dipole tensor is the first of three sources of anisotropy that are often neglected in modelling diffusion of H. A second is the elastic anisotropy of Zr, with its five independent elastic constants. A third is anisotropy of the diffusion tensor in Zr, with its two independent diffusivities. So far we have included only the first two sources of anisotropy.

The equation of stress-driven diffusion becomes:

$$\frac{\partial c}{\partial t} = D\left[\nabla^2 c - \frac{\rho_{ij}}{k_B T}\left(\boldsymbol{\nabla} c \cdot \boldsymbol{\nabla}\varepsilon_{ij} + c\,\nabla^2\varepsilon_{ij}\right)\right], \tag{3}$$

where $D$ is the diffusion tensor of hydrogen in zirconium at temperature $T$. By representing $D$ as a scalar quantity we have ignored its anisotropy.

It is commonly assumed that the elastic stress can dictate where hydrides precipitate. Experiments on both DHC and hydride re-orientation under stress [15] show this behaviour. Hydrogen solubility curves, measured on relatively large volumes of material, also show that the solubility limit is of the order of 1 wppm at room temperature [2]. One may therefore conclude that in-service stresses may increase the global concentration enough to trigger the hydride precipitation. This description is unfortunately too simplistic at the microscale. As it will be explained later, the stoichiometry of the hydride combined with the time-scale of precipitation suggests that the *local* hydrogen concentration has to be much higher than 1 wppm. This is valid at the scale of nanometres, associated with an individual nano-hydride precipitation event. Indeed, DFT calculations show that below concentrations as high as 300 wppm, there is no thermodynamic driving force for precipitation of γ or δ phases [20]. We embrace the view in [20] that the local hydrogen concentration has to be greater than what is experimentally observed by global measurements. Thus, we have to use much higher stresses in our calculations to reach this range of concentrations. We assume that the background concentration is 100 wppm, and that the solvus is at 750 wppm. As our model does not include a fracture initiation criterion, this artificial stress does not have any other effect. Even at these concentrations, the assumption of the dilute solution is still considered to be a valid one. On the grounds of DFT simulations [20], the H-H interactions are small and of the order of $10^{-2}$ and $10^{-3}$ eV at concentrations of about 580 and 75 wppm respectively. When compared with thermal fluctuations that are of about $2.5 \cdot 10^{-2}$ eV at room temperature, the interaction energy will play a role only at the highest values in our simulations.

The hydrogen concentration profile can be propagated in time using numerical algorithms to solve equation 3

such as the Crank-Nicholson scheme. Diffusion of hydrogen is fast, due to its small size and interstitial character. In typical reactor conditions (600 K) it diffuses at a rate of about 1 mm/hour [2]. To start the simulation the equilibrium hydrogen concentration is calculated with the analytic elastic field of a loaded crack or notch for a given hydrogen concentration $c_0$ far from the crack. In normal reactor conditions, the total H concentration in the alloy can range from ∼10 ppm at the start of life to ∼600 ppm at the end. This is a *global* figure, which takes into account both the hydrogen in solid solution and that inside the hydrides. For an elastic strain field $\varepsilon_{ij}(\mathbf{x})$ the equilibrium hydrogen concentration profile is given by:

$$c(\mathbf{x}, T) = c_0 \exp\left[\frac{\rho_{ij}\varepsilon_{ij}(\mathbf{x})}{k_B T}\right]. \tag{4}$$

We treat the diffusion of hydrogen and the precipitation of microhydrides as distinct processes with distinct length and time scales, adopting a systematic sequential multiscale modelling approach in time. We assume the elastic field is constant until a microhydride is precipitated, and the hydrogen concentration reaches equilibrium according to equation 4. The time taken for this process is of order hours, and the characteristic length is of the order of millimetres. Once hydride precipitation has occurred the characteristic length (∼µm) becomes much shorter because the reaction becomes autocatalytic, as discussed below. The exact mechanisms of the formation of microhydrides are not known [2], but three things must happen more or less in sequence. Prior to precipitation, hydrogen must diffuse and reach a threshold concentration. At this stage the hydrogen is in solid solution and its diffusion is governed by equation 3. A solid solution concentration of 100 wppm corresponds to an occupancy ratio of the tetrahedral sites of about 9:1000. Secondly, hydrogen must cluster very locally, as the occupancy ratio is about 1:2 for the γ phase and about 1.5:2 for the δ phase. Thirdly, the clustering must lead very swiftly to precipitation of a microhydride as otherwise the H-H repulsion in a solid solution of Zr will drive the hydrogen atoms apart [35]. Hydrogen behaves as a negatively charged ion, screened by Zr atoms due to the large difference in electronegativity of H (2.2) and Zr (1.3). During this final step zirconium atoms most likely undergo a displacive rearrangement from the hexagonal to the cubic or tetragonal structure of the microhydride, which we assume occurs in a negligible time compared to other timescales of interest. The temporal sequence in the model is: (i) long-range transport of H to the loaded notch as modelled by our stress-driven equation; (ii) mid-range clustering of H atoms to localised nucleation sites that is not explicitly modelled here; (iii) short-range martensitic reconfiguration of the Zr atoms and reordering of the H atoms as the solid solution transforms into a hydride phase, which is also not explicitly modelled.

Hydrogen diffusion occurs over much longer length and time scales than the precipitation reaction. The length-scale of the precipitation is that of a single microhydride, i.e. ∼1 µm. Thus diffusion of hydrogen and precipitation of a microhydride may be decoupled in space and time. To achieve this decoupling in the simulation the resolution of the spatial mesh must not be finer than a single microhydride. When the microhydride is precipitated it is then fully formed. Diffusion and precipitation are"decoupled" in the sense that the relevant phase variables are not bound together in the same set of partial differential equations (i.e. like in PF or FE models) but these two processes are still algorithmically coupled and the algorithmic diffusion-precipitation framework takes into account the physical time scales to alter (but not eliminate) the coupling so that the computational model is efficient. It is a key feature of our model that diffusion and precipitation are decoupled processes. The former is treated at a continuum level using analytic solutions for the elastic field, and the latter is treated within a discretised and spatially localised framework. This is different from PFM where the growth of a microhydride is modelled incrementally in both space and time. In PFM fewer such microhydrides can be treated in the simulation, owing to the computational cost associated with the much finer length and time scales treated in these models.

## 2.2 The dislocation dipole representation of a microhydride

The experimental evidence reviewed in the previous section leads us to model the microhydrides as narrow elliptical discs, the major axes of which are parallel to one of the three $\langle 11\bar{2}0\rangle$ directions. The elastic fields of the microhydrides result from the coherent nature of their interfaces and the transformation strains, which are constrained by the surrounding matrix. The elastic field of the microhydride may be represented by a continuous distribution of edge dislocations with infinitesimal Burgers vectors. This continuous distribution maintains continuity of displacements and tractions at the interface of the microhydride once the region occupied by the microhydride has transformed [36]. In a two-dimensional representation parallel to the basal plane let $\beta(x, y)$ denote the density of Burgers vector per unit length on the interface where $x$ is along $\langle 11\bar{2}0\rangle$ and $y$ is along $\langle 1\bar{1}00\rangle$. According to Carpenter et al. [4], $\varepsilon_{11\bar{2}0} \sim 0.1\varepsilon_{1\bar{1}00}$. Hence, the Burgers vector density $\beta_y$ along $y$ is an order of magnitude less than $\beta_x$ along $x$. Therefore, we ignore the small Burgers vector density along $y$ and consider only the Burgers vector density along

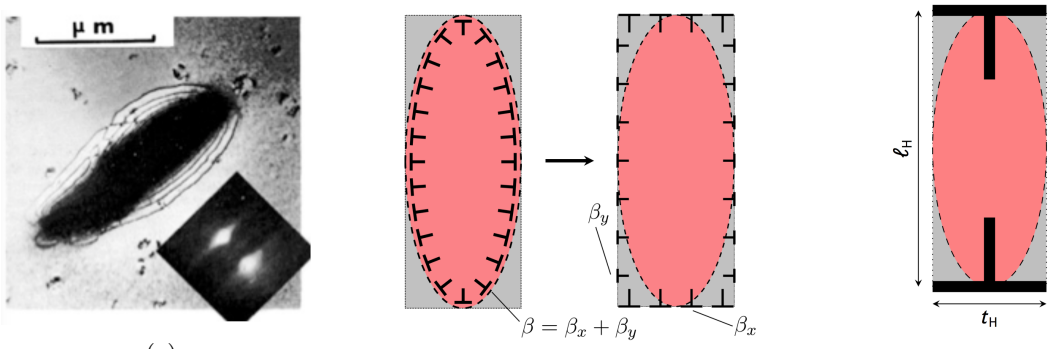


(a) (b) (c)

Figure 2: (a) TEM micrograph of a microhydride from Ref. [4]. (b) There is a continuous distribution of infinitesimal dislocations with Burgers vector density $\beta = \beta_x + \beta_y$ in the interface of the elliptical microhydride ($x$ is horizontal in this figure and $y$ is vertical). The transformation strain ensures $\beta_y \ll \beta_x$. As the aspect ratio $l_H/t_H$ increases the faces along $y$ come closer together and the faces along $x$ move further apart. The relatively small value of $\beta_y$ in combination with the close proximity of the faces along y enable us to ignore the dislocations in those faces. As the aspect ratio $l_H/t_H$ increases the Burgers vector density $\beta_x$ is concentrated increasingly in the small faces along x. It is then a good approximation to replace the continuous distribution of infinitesimal dislocations surrounding the microhydride with a single dipole of discrete edge dislocations at the top and bottom with Burgers vectors $\pm\varepsilon_{1\bar{1}00}t_H$.

$x$. This approximation improves as the aspect ratio $l_H/t_H$ increases because the dislocations in the opposing faces along $y$ then screen each other much more than those in the opposing faces along $x$. In addition, as the aspect ratio $l_H/t_H$ increases the Burgers vector density parallel to $x$ is concentrated increasingly at the two ends of the microhydride. In that case it is a good approximation to replace the continuous distribution of dislocations around the microhydride by a single dipole of edge dislocations with Burgers vectors $\pm\varepsilon_{1\bar{1}00}t_H$, as illustrated in Fig.2c. This limits our attention to the γ phase. In this way the elastic field of each microhydride is represented analytically, even in anisotropic elasticity, which is a further major simplification of our treatment. *For instance, the stress field of a γ hydride growing from a nucleation site at $(x_H, y_H)$, and oriented as the one in Fig.2c, is given by:*

$$\sigma_{xx} = \frac{\mu\varepsilon_{\langle 1\bar{1}00\rangle}t_H}{2\pi(1-\nu)}\left[\frac{(y-y_H-l_H/2)\left(3(x-x_H)^2+(y-y_H-l_H/2)^2\right)}{\left((x-x_H)^2+(y-y_H-l_H/2)^2\right)^2} - \frac{(y-y_H+l_H/2)\left(3(x-x_H)^2+(y-y_H+l_H/2)^2\right)}{\left((x-x_H)^2+(y-y_H+l_H/2)^2\right)^2}\right] \tag{5}$$

$$\sigma_{yy} = \frac{\mu\varepsilon_{\langle 1\bar{1}00\rangle}t_H}{2\pi(1-\nu)}\left[\frac{(y-y_H+l_H/2)\left((x-x_H)^2-(y-y_H+l_H/2)^2\right)}{\left((x-x_H)^2+(y-y_H+l_H/2)^2\right)^2} - \frac{(y-y_H-l_H/2)\left((x-x_H)^2-(y-y_H-l_H/2)^2\right)}{\left((x-x_H)^2+(y-y_H-l_H/2)^2\right)^2}\right] \tag{6}$$

$$\sigma_{xy} = \frac{\mu\varepsilon_{\langle 1\bar{1}00\rangle}t_H}{2\pi(1-\nu)}\left[\frac{(x-x_H)\left((x-x_H)^2-(y-y_H+l_H/2)^2\right)}{\left((x-x_H)^2+(y-y_H+l_H/2)^2\right)^2} - \frac{(x-x_H)\left((x-x_H)^2-(y-y_H-l_H/2)^2\right)}{\left((x-x_H)^2+(y-y_H-l_H/2)^2\right)^2}\right] \tag{7}$$

*Here, $\mu$ is the shear modulus and $\nu$ is the Poisson's ratio for Zr. $x$ is along $\langle 1\bar{1}00\rangle$ and $y$ is along $\langle 11\bar{2}0\rangle$.* Note that the matrix above and below the microhydride in Fig. 2c is in the tensile fields of the edge dislocations. This is what leads to the autocatalysis, i.e. the next microhydride is most likely to be precipitated in one of these tensile regions. The elastic interactions between edge dislocations in adjacent microhydrides explains their stacking in a macrohydride. *In order to demonstrate the validity of the dipole approximation, in App. A the stress field of a γ hydride was plotted in the three cases considered in Fig. 2, i.e. assuming an elliptic distribution, a rectangular one or the dipole approximation.*

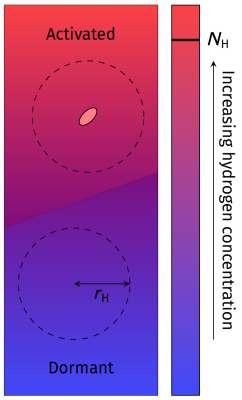


Figure 3: The randomly distributed nucleation sites are activated or dormant depending on the local hydrogen concentration.

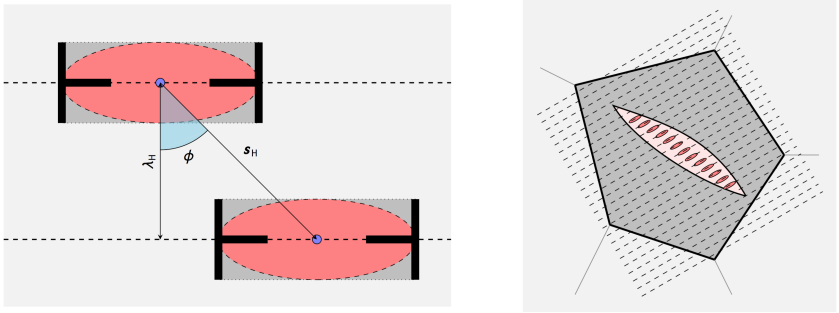


(a) (b)

Figure 4: (a) In the autocatalytic nucleation process, a second microhydride nucleates close to the first to reduce the total elastic energy compared to when the two microhydrides are well separated. Its exact location is decided by minimising the total elastic energy with respect to the parameter $\phi$. (b) Schematic representation of how the shape and habit plane of a macrohydride results from the stacking of microhydrides within it. Dashed lines represent basal planes.

## 2.3 Microhydride precipitation

We describe in this section where and when microhydrides can be created. Zircaloy-2 and Zircaloy-4, like other Zr-alloys, contain intermetallic second phase particles (SPPs) [37, 38]. To ensure good corrosion behaviour, it is desirable to have a fine dispersion of these SPPs [38]. They are potential sites for heterogeneous nucleation of hydrides within grains [39]. For example, hydrides nucleating at intermetallic particles are seen in Fig. 1 of Ref. [4]. Other defects may provide sites for heterogeneous nucleation, such as irradiation-induced $c$-type dislocation loops [9]. For these reasons we have so far assumed nucleation sites are randomly distributed within the simulation cell. We have not considered intergranular precipitation in this initial conceptual model, but this is a relatively straightforward extension.

As already discussed, the nucleation of a microhydride requires sufficient hydrogen to be present in a region substantially larger than the microhydride itself. This is tested by integrating the hydrogen content over a circle of radius $r_H$ centred on the nucleation site, as schematically shown in Fig. 3. This hydrogen content is compared to the number of hydrogen atoms required to create a hydride ellipse with an area of $\pi l_H t_H/4$. The variables $r_H, l_H, t_H$ are input parameters of the model. It is worth repeating that, given the stoichiometric equivalence that must be satisfied, a substantial amount of hydrogen has to be clustered around the precipitating but still pure zirconium phase. If this approach were applied under the assumption of a solubility limit of 1 wppm, hydrogen would have to gather very quickly from a volume about 11,000 times larger than the hydride. This looks unrealistic, given the distances observed between microhydrides, and hints at the fact that locally the hydrogen concentration has reached much higher values, as suggested by DFT [20].

Once the nucleation site is activated, the microhydride could appear on any of the three $\langle 11\bar{2}0\rangle$ directions in the Zr basal plane. The direction selected is that which minimises the global elastic energy, for which we have derived analytic expressions.

From the experimentally observed staircase-like appearance of the microhydrides within a macrohydride, it can be inferred that the precipitation follows an autocatalytic process that we simulate as follows. An additional nucleation site is introduced in the proximity of every site that has become active. Its location is determined by minimising the total elastic energy with respect to the parameter $\phi$ defined in Fig. 4a. The parameter $\lambda$, also defined in Fig. 4a, is an input parameter. Following the creation of the first microhydride the new equilibrium hydrogen concentration field is calculated using equation 4. Alternatively, the hydrogen concentration can be evolved in time using equation 3 with an appropriate boundary condition at the border of the simulation cell. The simplest boundary condition is that there is no flux into or out of the simulation cell anywhere on its border. This is acceptable provided the cell is sufficiently large. If there is enough hydrogen in solution in a circle of radius $r_H$ centred on the new nucleation site a second microhydride is introduced. And so the process can continue, with the macrohydride lengthening by the autocatalytic nucleation of further microhydrides, until a grain boundary is reached. It can continue on the other side of the grain boundary but with a change of orientation because the orientation of the $a$-axes changes. In this way the simulation of the formation of a macrohydride comprising a stack of microhydrides can proceed remarkably rapidly. The autocatalysis is captured naturally through the minimisation

of the total elastic energy and the representation of each microhydride as a dislocation dipole, which favours the resulting habit planes for the macrohydride close to those observed experimentally. Perhaps more significantly, the minimisation of the global elastic energy reproduces the experimentally observed reorientation of macrohydrides beneath stressed cracks and notches. Fig. 4b illustrates the staircase arrangement within a macrohydride inside a grain.

## 2.4 Initialising the simulation

The model currently runs on a 2.9 GHz workstation with 2 GB memory. It simulates the precipitation of hydrides around a notch subjected to a remotely applied load. There are a series of four steps to initialise the simulation, which are described here and illustrated in Fig. 5.

First, the two-dimensional simulation cell is defined. It is a rectangular region with sides parallel to the $(x, y)$ axes of a Cartesian coordinate system. The sides along $y$ have length 2 mm, and those along $x$ have length 1 mm. The origin of the coordinate system is at (0,1) mm. An elliptical notch is introduced. It is centred at the origin and is described by the equation $(x/a)^2 + (y/b)^2 = 1$, where $a$ and $b$ are the semi-axes. The ellipse is very versatile. It can describe both blunt, circular notches ($a = b$) and sharp notches ($b \ll a$).

Second, the simulation cell is meshed for the evaluation of the elastic and hydrogen concentration fields. There are $n_x$ and $n_y$ mesh points along the $x$ and $y$ dimensions respectively, such that the grid spacing is $\Delta l_x = 1/n_x$ mm and $\Delta l_y = 2/n_y$ mm. The smallest physical dimension in the model is the microhydride needle of 1 µm. Accordingly, $n_x = 1000$ and $n_y = 2000$.

Third, the grain structure of the zirconium alloy is created. This is achieved using a two-dimensional Voronoi tessellation of convex polygons. This computational geometry technique has been frequently used in computational metallurgy [40], to create grain structures produced by normal grain growth. A set of random points, known as seeds, is defined in the simulation cell, with an areal density to match the desired average grain size. The Voronoi construction is then performed on these points to divide the simulation cell into convex polygons separated by straight lines that become grain boundaries. Each grain is assigned a randomly chosen rotation about the $c$-axis, and the orientation of the grain is assigned to all mesh points that fall within it. In this way we simulate a polycrystal with a [0001] texture.

Fourth, initial nucleation sites are placed randomly inside the simulation cell. Two parameters characterise nucleation sites in our model: (i) the average number of nucleation sites per grain $\rho^{(\alpha)}$, and (ii) the radius $r_H^{(\alpha)}$ of the circular region centred on each nucleation site that is depleted of hydrogen to enable a microhydride to be formed fully at the nucleation site. Mesh points that belong to each nucleation site are identified and stored. In reality a variety of nucleation sites is expected, with a range of thresholds for activation. This can be simulated by having a variety of radii $r_H^{(\alpha)}$, with larger values corresponding to sites with a lower activation threshold.

We require the elastic field of an infinitely long elliptical or V notch in a semi-infinite medium loaded in mode I or mode II. It has to be calculated only once at the beginning of the simulation. Finite elements are avoided because we want a fast code that ultimately can be run on minimal computational needs with different notch geometries, grain microstructures and textures, nucleation site densities following different irradiations, and so on. We also want the code to be able to be run repeatedly with different microstructural variables to create ensemble averages

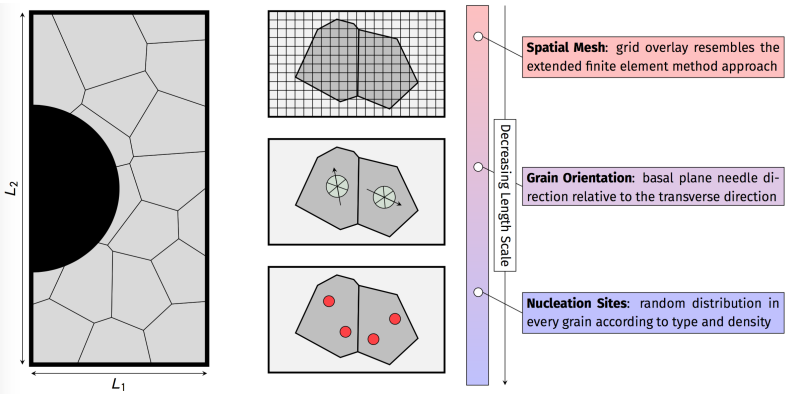


Figure 5: Left: the simulation cell with a circular notch (grain size exaggerated for clarity). Right: outline of the steps for the initialisation of the simulation.

of thousands of instances. Finite element simulations are considered too cumbersome for these requirements. By choosing a simple geometry we can use analytic solutions instead. Two analytic approaches exist: the method of conformal maps and Muskhelishvili's complex potentials (e.g. Lazzarin and Tovo [41]), and the technique of distributed dislocations (e.g. Nowell et al. [42]). The distributed dislocation technique is preferable at present because (i) the conformal mapping creates non-trivial inter-dependencies between geometrical parameters that describe the V- and U-notches; (ii) we do not need the sextic roots needed in the Stroh/Lekhnitskii formalism - rather we have analytical solutions of the dislocations in hexagonal media so we only need a one-off computation of the dislocation distribution function.

## 2.5 Architecture of the code

The code is structured in three nested loops. The outer loop (1A, time iteration loop) is run over time to evolve the concentration field as microhydrides precipitate. At each timestep the code loops over all nucleation sites and checks whether there is enough hydrogen for a microhydride to be introduced (1B, nucleation loop). At each activated nucleation site the innermost loop determines the orientation of the microhydride needle, which is then introduced, and an adjacent nucleation site (2A-3B, macrohydride loop) is introduced to simulate the possibility of autocatalysis. A flowchart is presented in Fig. 6 and comprises the following steps:

1A) *Concentration mesh iteration.* The hydrogen profile is updated at each mesh point according to equation 3 or 4.

1B) *Nucleation activation criterion.* The amount of hydrogen around each nucleation site is calculated by integrating the concentration profile. The nucleation site is activated if the precipitation criterion is met.

2A) *Computational geometry check.* Allowed microhydride configurations are checked using computational geometry.

2B) *Addition of precipitates.* If the proposed location of the microhydride is permissible, the microhydride is introduced, and an additional nucleation site is inserted in its vicinity.

2C) *Diffusible solute correction.* The hydrogen which is now in the hydride is removed from the diffusible hydrogen of the system, according to the stoichiometry of the precipitation.

3A) *Needle configuration evaluation.* The habit plane of the needle is decided after sampling the three possible basal $\langle 11\bar{2}0 \rangle$ directions, to find the one having the lowest energy.

3B) *Stress state update.* The global elastic field is updated to include the fields created by introduced microhydrides using the superposition principle of linear elasticity.

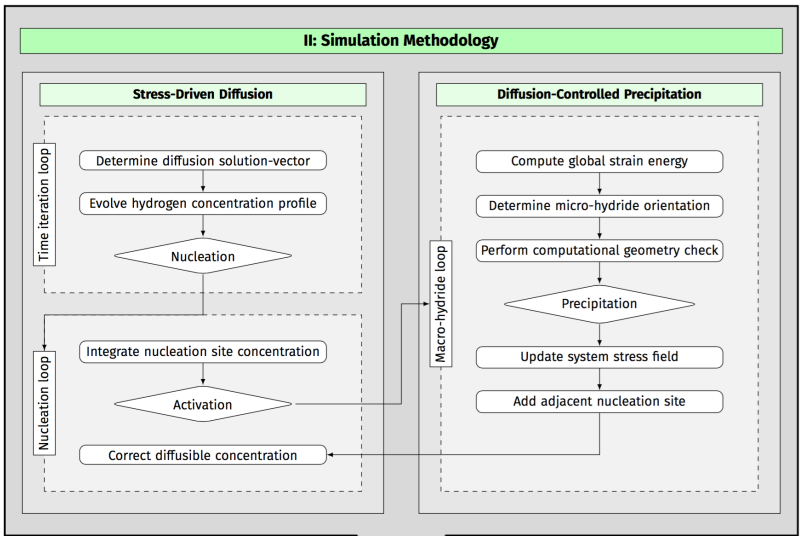


Figure 6: Flowchart of the simulation methodology for connecting the diffusion and precipitation analyses, with three nested loops. The first concerns the stress-diffusion analysis. The second loop is over the nucleation sites, which are randomly distributed inside all the grains. The third loop implements the autocatalytic mechanism.

Point 2A highlights an important feature of the implementation. The code uses optimised computational geometry algorithms to determine the allowed configurations of microhydrides. In particular, the two families of algorithms of interest are the polygon-line segment intersection (PLSI) and the line-segment intersection (LSI). This ensures that the platelets of a growing macrohydride, upon crossing a GB, assume the correct orientation imposed by the crystallography of the neighbouring grain. More details about them and their implementation are beyond the scope of this paper, and will be published elsewhere in future. The key to the extremely fast computations resides in the combination of analytical expressions for the stress state, the assumption of the equilibrium solution of the diffusion equation and the usage of computational geometry.

## 2.6 Assumptions and limitations

Here we list the principal assumptions and limitations of the model:

- The model uses plane strain elasticity and is therefore two-dimensional. However, the Zr-cladding is a cylindrical shell of axial length of the order of metres, and thickness of the order of millimetres. With the assumption that the notch runs along a considerable length of the cladding the plane strain approximation is not unreasonable. Another consequence of the two dimensional nature of the model is that microhydrides are no longer needles but infinitely long columns with needle-like cross-sections. Similarly the hydrogen is no longer present as a single atom but as an infinitely long column of hydrogen atoms. These features hold for all two-dimensional microstructural models of similar type. Also related to its two-dimensional nature is the limitation of the model to address only [0001] textures. This limitation follows from the requirement that all three $\langle a \rangle$-directions of growth of the microhydrides must be accessible in the simulation and therefore they must lie in the plane of the simulation cell. It would be an understatement to say that turning this model into a full three-dimensional treatment would be a formidable undertaking. Having said this, devising a 3D version would be, conceptually, not such a stretch from the current framework. There are known analytical and semi-analytical solutions to three-dimensional elastic fields (even in anisotropic elasticity e.g. [43]) and point-in-a-polygon algorithm would be replaced by a point-in-a-polyhedron algorithm (which is again very fast as most video games are real-time fast using 3D graphics engines), and Polyhedron-LSI and LSI would now be in 3D. Even in the 3D conceptualisation the computational complexity would still only scale with the number of hydrides (if hydrides were geometrically represented by a straight line but in a three-dimensional space).
- The dislocation dipole approximation assumes $\varepsilon_{\langle 11\bar{2}0\rangle} \ll \varepsilon_{\langle 1\bar{1}00\rangle}$. This is a valid assumption in the case of the $\gamma$ hydride. But when the $\delta$ phase arises, e.g. during slow cooling and at higher hydrogen concentrations [44], the assumption may no longer be valid. In particular, the strains reported in Ref. [7] would invalidate the assumption, whereas those reported in Ref. [8] would tend to support it.
- The elastic fields are calculated using analytic expressions. This limits the choice of the notch geometry. However, experimental studies of DHC or of hydride reorientation usually involve either U- or V-notches, for which analytic expressions do exist.
- Plasticity has not been implemented in the model. It could be important in both shielding the field of a notch, which would reduce the attraction of hydrogen to its root, or indeed in reattracting H trapped by edge type dislocation strain fields. In a preliminary, exploratory study plasticity was introduced using discrete dislocation plasticity in a submodel [45] to investigate plastic relaxation around macrohydrides and their possible influence on thermal ratchetting.
- We have ignored H-H interactions, because these are short-ranged, in modelling stress-driven diffusion of hydrogen. These interactions become significant at higher hydrogen concentrations. We find that to achieve sufficiently high concentrations of hydrogen to nucleate microhydrides we have to apply unrealistically high loads to notches. This suggests that the model needs a proper description of heterogeneous nucleation. *There is also no influence of the H is solid solution on the stress fields of the dislocations that represent the hydride. However, we believe this to be a second-order effect. Moreover, dislocations are used here not as crystallographic entities but as sources of stress. Hence this effect may be indirectly incorporated through the parameter $t_H$, provided that it could be quantitatively estimated.*
- The separation between hydrogen diffusion and hydride precipitation is based on the difference between length and time scales involved in the two processes. Of course in reality microhydrides do not appear fully formed but grow from a nucleus through further diffusion of hydrogen across the interface between the hydride and the surrounding matrix. This is reproduced reasonably well in other models but at significant computational

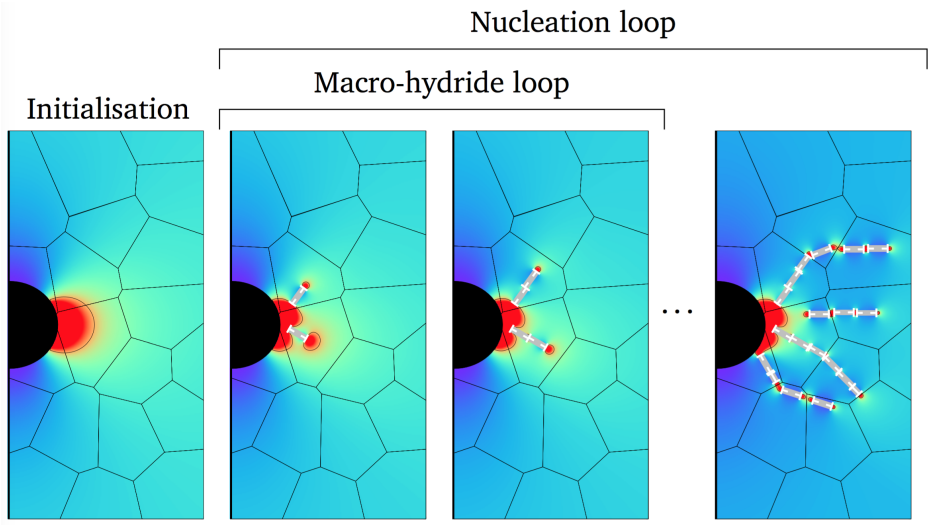


Figure 7: Snapshots from a simplified simulation showing how the network of hydrides spreads from the root of the notch loaded in tension with the tensile axis vertical. Time increases from left to right. Note the hydrides start in a radial arrangement at the notch root, and tend to align themselves perpendicular to the loading direction further from the notch. Colour scale shows hydrogen concentration red (high) to blue (low).

cost. With the goal of modelling hydrided microstructures at much larger length scales we have to ask whether this more accurate treatment of diffusion and precipitation is worth the computational penalty.

- The model currently assumes that the temperature is constant throughout the simulation cell. In reality hydrogen transport is influenced by thermal gradients. Thermal gradients and the overall temperature also influence stresses through the anisotropic thermal expansion tensor of Zr, and the different thermal expansion tensor of the hydrides.
- A particularly important limitation when anisotropic elasticity is used is the neglect of compatibility stresses at grain boundaries. These can be as large as any other stresses present in the model, and they are very difficult to include without the use of finite elements. One possibility is to include a one-off crystal plasticity finite element calculation. But the aim is again to reproduce the observed microstructures and, if this can be done without the explicit need for compatibility corrections to the system (and it probably can through some more microstructural data and conclusions drawn from EBSD maps and SEM/TEM findings), then it would be a far more efficient computation that can easily accommodated within the framework that we have proposed.

# 3 Results and discussion

The simulations presented in this section assumed the sample is at room temperature and that the remote H concentration is 100 ppm. The material is polycrystalline with a [0001] texture, and the grain rotations about [0001] are random. In these demonstrating simulations there is only one nucleation site per grain. This is for computational simplicity, as it means that the macrohydrides do not interact and the number of computational geometry checks decreases. It is the addition of nucleation sites during the autocatalytic precipitation that ensures the growth of the macrohydride.

First, we present in Fig. 7 an initial, simplified model used for testing key features. The simplification is that instead of macrohydrides comprising a stack of microhydrides, the macrohydride is a single entity represented by a single “super-dipole”, shown in white in the figure. This is not a simplification one would normally use because it does not capture the finer scale reorientation of the macrohydride that microhydrides allow. It should also be noted that the grain size is exaggerated, again for purposes of illustration. Despite these simplifications, the principal features of experimental micrographs are reasonably well captured. The hydrides begin to precipitate at the root of the notch, in a radial fashion. They can continue, with a break, on the other side of GBs. With increasing distance from the notch they tend to lie perpendicular to the tensile axis, as expected.

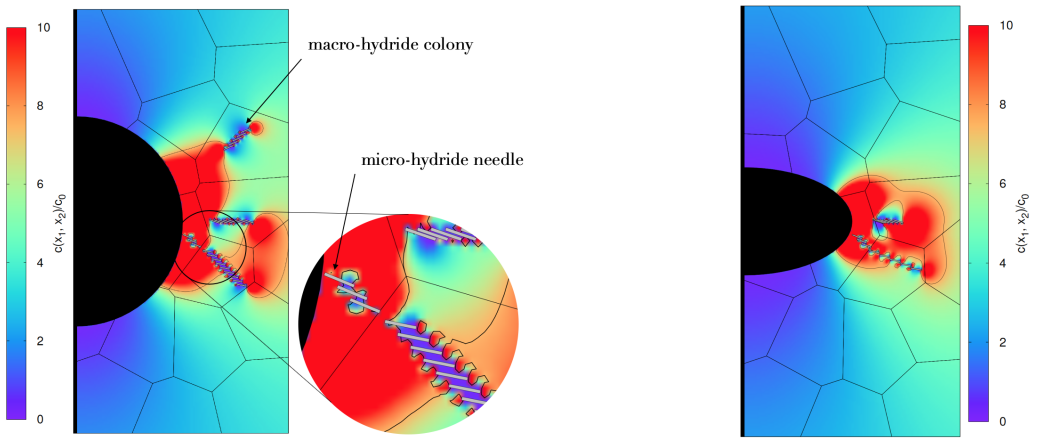


(a) (b)

Figure 8: Simulated micrographs superimposed on the calculated H concentration profile, showing the effect of the notch sharpness for the same tensile load and the same polycrysalline structure. (a) Blunt circular notch showing a radial arrangement of hydrides. The inset shows the stacking of the microhydrides in greater detail and how the macrohydride is stopped at the GB and restarted on the other side. (b) Hydrides formed at the root of a sharper elliptical notch. Although the orientation of the macrohydride habit plane is the same in the grain nearest to the notch tip as in (a), it differs from (a) on the other side of the grain boundary. The grain size was enlarged to 500 µm and the microhydrides were enlarged to 50 µm to make the images clearer. The colour bar is the same for the two images.

We then present in Fig. 8 the initial attempts to model the microstructures generated growing the macrohydride as a collection of autocatalytically nucleated stacks of microhydrides. The first example illustrates the influence of the notch acuity. It is instructive to display the hydride network superimposed on the H concentration profile. The grain size was increased to 500 µm and the microhydride needles increased in length to 50 µm to aid visualisation. The grain size and the microhydride length were returned to values closer to reality for a comparison with experimental results below.

The inset in Fig. 8a shows the deck-of-cards stacking that is visible in TEM images of macrohydrides [10]. In the case of the circular notch ($a = b = 500$ µm, Fig. 8a), three sites were activated, one of which was relatively far from the notch tip. In the sharper, elliptical notch ($a = 500$ µm, $b = 250$ µm, Fig. 8b) two sites became active under the same applied stress, both close to the notch tip. In both examples, the precipitation did not start at the surface of the notch. The macrohydride stops at the grain boundary and restarts on the other side, adopting a slightly different orientation as expected. The images show the expected local depletion of H that results from the formation of hydrides. Growth of the macrohydrides stops when the stress is insufficient to attract sufficient hydrogen to nucleate further microhydrides.

The simulation in Fig. 8a took less than 10 s to run on a workstation with a 2.9 GHz processor and 2 GB RAM capacity.

We compared the model with experimental images, selecting a closer to realistic average grain size of 50 µm for comparison with the optical micrographs by Cui et al. [46]. The output of our model is shown in Fig.9 alongside images from Ref. [46]. The area of the simulation cell is the same size as that of the optical micrographs. To improve visualisation, the length of the microhydrides was set to 5 µm, as it was found that the overall simulation was not seriously affected.

In Fig. 9a the model predicts the spreading of a densely populated hydride network from a sharp elliptical notch. This agrees with several macrohydrides that precipitated at the root of the V-notch in Fig. 9c. Fig. 9b reproduces quite well the radial pattern of macrohydrides around circular notches seen in Fig. 9d. It is easy to see that the first case is a greater concern than the second from the standpoint of structural integrity.

For the simulations in this section, the notch was subjected to a very high stress of 140 GPa. This was necessary to raise the H concentration sufficiently at the notch to nucleate microhydrides. Of course, no metal could be able to withstand such a stress. However, as we are considering the local H concentration, similarly the stress should be thought of as a local one, which at the microscale features such as GBs can reach the range of GPa, as experimentally measured with e.g. electron backscatter diffraction [47].

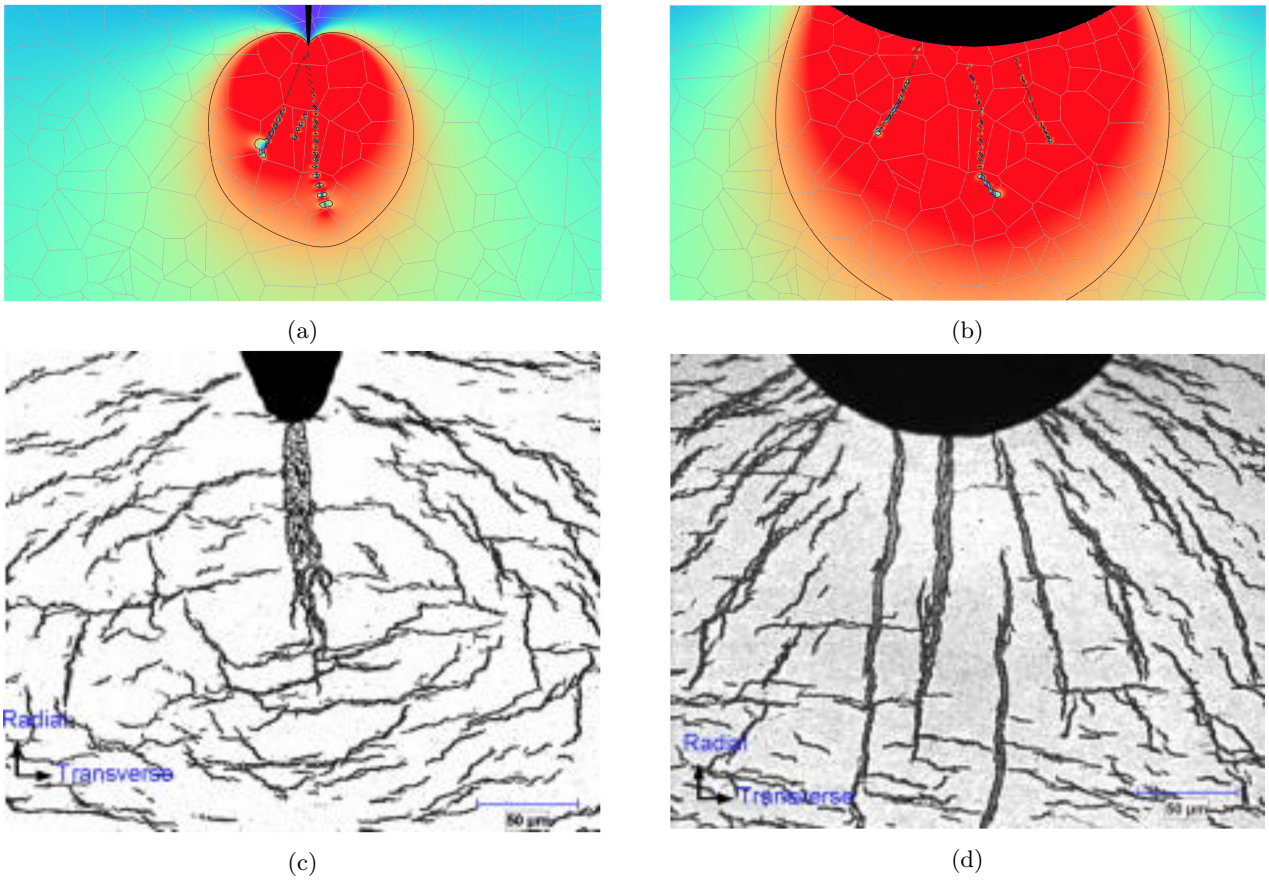


Figure 9: Comparison between the simulated micrographs (for which the colour bar is the same as in Fig. 8) and the experimental micrographs by Cui et al. [46]. Although not apparent due to the large system size, the macrohydride features are modelled as stacks of microhydride needles.

# 4 Conclusions and future directions

In this work we have sought to address the industrial need for a strategy for modelling hydride precipitation and reorientation that can rapidly simulate much larger length and time scales than current existing computational models. We believe our work has provided the first realistic simulations of hydrided microstructures at the millimetre scale. This has been achieved through a set of assumptions designed to simplify the problem computationally while retaining as much as possible the essential physics. It has been essential to use theoretical elasticity to avoid being encumbered by the computational cost of finite element simulations. The result is a very fast and efficient multiscale model, able to bring the fine micrometric structure of the microhydrides into a simulation of a notched component at the millimetre scale containing hundreds of grains.

Some of the simplifications we have made were computational, such as the deliberate avoidance of finite element techniques by using analytic expressions for elastic fields of loaded notches. Some of them were physical such as representing the elastic field of a microhydride by a dislocation dipole. We treated hydrogen diffusion and microhydride precipitation as sequential events rather than simultaneous events. In common with many models in materials science, we treated the problem only in two dimensions. In the development of any strategy for modelling choices always have to be made, which may compromise the treatment of the physics of the problem. The challenge is to find an optimum trade-off between meeting engineering requirements and treating as accurately as possible the physics of the problem. By maintaining a rigorous balance between these competing demands we believe we have laid the foundations of a new way of modelling that will meet the needs of colleagues in industry. Our framework should not be seen as an alternative to existing models, but rather as a tool to complement them. In fact, the ability of our model to simulate realistic microstructures in a remarkably short time immediately makes it possible to envisage ensemble averaging by treating different random arrangements and potencies of nucleation centres. Vital sensitivity studies can be carried out routinely to identify the most important factors controlling hydride precipitation and reorientation, such as grain size, SPP content, notch acuity, temperature, yield strength, and so

on. A great many combinations of them could be scanned, and slower existing models could be applied only to the handful of cases deemed most critical. We also use computer vision to simulate most of the foundational physics of the hydride precipitation as observed in experiments: hence this opens up the gateway to machine learning techniques that constitute the frontiers of the intersection of the computational and computer science.

There are many ways in which the model may be improved. A hierarchy of heterogeneous nucleation sites could be included e.g. at grain boundaries. These sites are likely to be very significant, especially since crystal plasticity simulations showed that thermal residual stresses can induce H segregation and hydride nucleation at the GB [48]. The model could be developed further to model the thermal ratchetting effect. There is experimental evidence that hydride precipitation causes plastic deformation in the surrounding matrix with the generation of both $a$-type dislocations [4, 8] and $c$-type dislocations [49]. It is likely that not all these dislocations disappear during reheating to 300 ℃ that redissolves the hydrides. These dislocations may then act as nucleation sites for hydrides when the material returns to normal service, thus providing a "memory effect" [50] in the sense that hydrides precipitate in the same places as the previous set of precipitates. This would require an expansion of the work started by Patel et al. [45].


## Acknowledgements

This work was supported through a studentship in the Centre for Doctoral Training on Theory and Simulation of Materials at Imperial College London funded by the EPSRC (EP/G036888/1 and EP/L015579/1) and through an industrial collaboration with Rolls-Royce plc.


## Author contributions

M.P. wrote the computer code, developed the model and produced the figures. L.R. wrote the initial manuscript and helped interpreting the results. D.S.B, A.P.S. and M.R.W. supervised the project and helped with the development of the model. All authors co-wrote the final manuscript.

## Competing Interests

The authors declare that there are no competing interests.

## Data availability

The raw and processed data required to reproduce these findings cannot be shared at this time due to legal reasons.

## A The dipole approximation

One of the key points of the proposed multi-scale model is that the stress field of a $\gamma$ hydride can be accurately approximated by that of an edge dislocation dipole. In order to show that this is the case, we take the $\sigma_{yy}$ component as an example, as this is much stronger than the $\sigma_{xx}$ component and contributes much more to the resulting H profile. Let us consider a hydride of length 1 µm and thickness 200 nm. In the most faithful representation, the stress of the hydride is given by two elliptic distributions of dislocations, to capture the $\varepsilon_{\langle 1\bar{1}00\rangle} = 5.6\%$ and $\varepsilon_{\langle 11\bar{2}0\rangle} = 0.6\%$ misfits respectively. Fig. A.1a shows the plot of the stress field if the two distributions are discretised using 200 dislocations. Alternatively, if the shape of the hydride is approximated by a rectangle, using 200 discrete dislocations for each of the two, now straight distributions, the $\sigma_{yy}$ stress is shown in Fig. A.1b. Finally, the plot of $\sigma_{yy}$ in Fig. A.1c exemplifies the dipole approximation: the misfit along $\langle 11\bar{2}0\rangle$ is neglected and two edge dislocations of Burgers vector $b = 0.056 \cdot 200$ nm are placed at the two hydride tips. These three representations match those schematically depicted in Fig. 2. They agree very well except within nm from the hydride itself. At distances of the order of µm, the three representations give analogous results as far as the proposed model is concerned. As already stressed in the main text, this approximation is good insofar as the misfit in one direction dominates that in the orthogonal one.

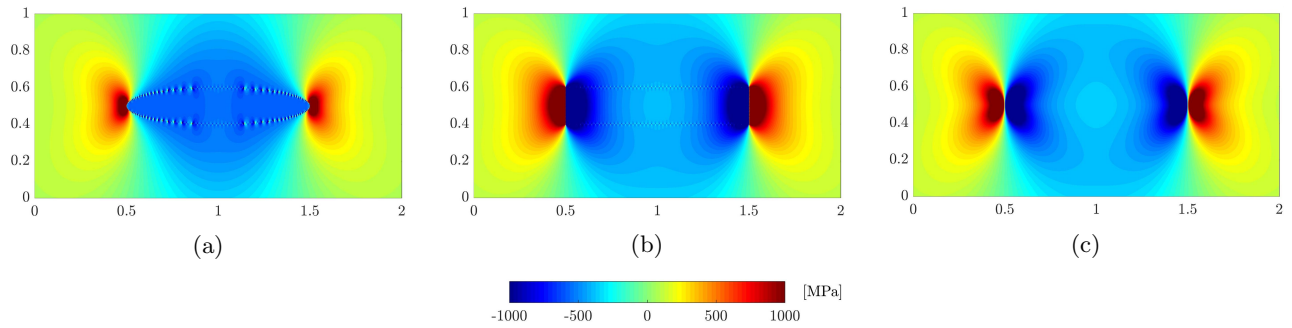


Figure A.1: The $\sigma_{yy}$ component of a $\gamma$ hydride of length 1 µm and thickness 200 nm is represented by distributions of edge dislocations. (a) 200 dislocations are placed in an elliptic distribution. (b) 200 dislocations are placed in a rectangular distribution. (c) A single dislocation dipole is used instead. Axes in µm. The horizontal direction is parallel to $\langle 11\bar{2}0\rangle$, the horizontal direction is parallel to $\langle 1\bar{1}00\rangle$.

# References


[1] S. Kass, "The development of the zircaloys," *Corrosion of Zirconium Alloys. ASTM International*, pp. 3–27, 1964.

[2] M. P. Puls, *The effect of hydrogen and hydrides on the integrity of zirconium alloy components: delayed hydride cracking*. Springer Science Business Media, 2012.

[3] J. Bair, M. Asle Zaeem, and M. Tonks, "A review on hydride precipitation in zirconium alloys," *Journal of Nuclear Materials*, vol. 466, pp. 12–20, 2015.

[4] G. J. C. Carpenter, J. F. Watters, and R. W. Gilbert, "Dislocations generated by zirconium hydride precipitates in zirconium and some of its alloys," *Journal of Nuclear Materials*, vol. 48, pp. 267–276, 1973.

[5] P. A. Olsson, A. R. Massih, J. Blomqvist, A. M. Alvarez Holston, and C. Bjerkén, "Ab initio thermodynamics of zirconium hydrides and deuterides," *Computational Materials Science*, vol. 86, pp. 211–222, 2014.

[6] J. S. Bradbrook, G. W. Lorimer, and N. Ridley, "The precipitation of zirconium hydride in zirconium and Zircaloy-2," *Journal of Nuclear Materials*, vol. 42, pp. 142–160, 1972.

[7] G. J. C. Carpenter, "The dilatational misfit of zirconium hydrides precipitated in zirconium," *Journal of Nuclear Materials*, vol. 48, no. 3, pp. 264–266, 1973.

[8] A. T. Barrow, A. Korinek, and M. R. Daymond, "Evaluating zirconium-zirconium hydride interfacial strains by nano-beam electron diffraction," *Journal of Nuclear Materials*, vol. 432, no. 1-3, pp. 366–370, 2013.

[9] H. Chung, R. Daum, J. Hiller, and M. Billone, "Characteristics of Hydride Precipitation and Reorientation in Spent-Fuel Cladding," *Zirconium in the Nuclear Industry: Thirteenth International Symposium*, pp. 561–561–22, 2002.

[10] V. Perovic, G. C. Weatherly, and C. Simpson, "Hydride precipitation in $\alpha/\beta$ zirconium alloys," *Acta Materialia*, vol. 31, no. 9, pp. 1381–1391, 1983.

[11] G. Han, Y. Zhao, C. Zhou, D.-Y. Lin, X. Zhu, J. Zhang, S. Hu, and H. Song, "Phase-field modeling of stacking structure formation and transition of $\delta$-hydride precipitates in zirconium," *Acta Materialia*, vol. 165, pp. 528–546, 2019.

[12] D. G. Westlake, "The habit planes of zirconium hydride in zirconium and zircaloy," *Journal of Nuclear Materials*, vol. 26, no. 2, pp. 208–216, 1968.

[13] A. T. Motta, L. Capolungo, L.-Q. Chen, M. Nedim, M. R. Daymond, D. A. Koss, E. Lacroix, G. Pastore, A. Simon, M. R. Tonks, B. D. Wirth, and M. A. Zikry, "Hydrogen in zirconium alloys : A review," *Journal of Nuclear Materials*, vol. 518, pp. 440–460, 2019.

[14] Y. S. Kim, S. B. Ahn, and Y. M. Cheong, "Precipitation of crack tip hydrides in zirconium alloys," *Journal of Alloys and Compounds*, vol. 429, no. 1-2, pp. 221–226, 2007.

[15] M. N. Cinbiz, D. A. Koss, A. T. Motta, J. S. Park, and J. D. Almer, "In situ synchrotron X-ray diffraction study of hydrides in Zircaloy-4 during thermomechanical cycling," *Journal of Nuclear Materials*, vol. 487, pp. 247–259, 2017.

[16] B. Christiaen, C. Domain, L. Thuinet, A. Ambard, and A. Legris, "A new scenario for ⟨c⟩ vacancy loop formation in zirconium based on atomic-scale modeling," *Acta Materialia*, vol. 179, pp. 93–106, 2019.

[17] Y. Zhang, X.-M. Bai, J. Yu, M. R. Tonks, M. J. Noordhoek, and S. R. Phillpot, "Homogeneous hydride formation path in a -Zr : Molecular dynamics simulations with the charge-optimized many-body potential," *Acta Materialia*, vol. 111, pp. 357–365, 2016.

[18] R. Khoda-Bakhsh and D. Ross, "Determination of the hydrogen site occupation in the $\alpha$ phase of zirconium hydride and in the $\alpha$ and $\beta$ phases of titanium hydride by inelastic neutron scattering," *Journal of Physics F: Metal Physics*, vol. 12, no. 1, pp. 15–24, 1982.

[19] C. Domain, R. Besson, and A. Legris, "Atomic-scale Ab-initio study of the Zr-H system: I. Bulk properties," *Acta Materialia*, vol. 50, no. 13, pp. 3513–3526, 2002.

[20] S. C. Lumley, R. W. Grimes, S. T. Murphy, P. A. Burr, A. Chroneos, P. R. Chard-Tuckey, and M. R. Wenman, "The thermodynamics of hydride precipitation: The importance of entropy, enthalpy and disorder," *Acta Materialia*, vol. 79, pp. 351–362, 2014.

[21] P. A. Burr, S. T. Murphy, S. C. Lumley, M. R. Wenman, and R. W. Grimes, "Hydrogen solubility in zirconium intermetallic second phase particles," *Journal of Nuclear Materials*, vol. 443, no. 1-3, pp. 502–506, 2013.

[22] M. Christensen, W. Wolf, C. Freeman, E. Wimmer, R. B. Adamson, L. Hallstadius, P. E. Cantonwine, and E. V. Mader, "H in $\alpha$ -Zr and in zirconium hydrides : solubility , effect on dimensional changes , and the role of defects," *Journal of Physics: Condensed Matter*, vol. 27, p. 25402, 2015.

[23] J. Blomqvist, J. Olofsson, A. M. Alvarez, and C. Bjerkén, "Structure and Thermodynamical Properties of Zirconium hydrides from first-principle." . Springer, Cham, 2011.," in *Proceedings of the 15th International Conference on Environmental Degradation of Materials in Nuclear Power Systems—Water Reactors*, pp. 671–681, Springer, 2011.

[24] Y. Udagawa, M. Yamaguchi, H. Abe, N. Sekimura, and T. Fuketa, "Ab initio study on plane defects in zirconium-hydrogen solid solution and zirconium hydride," *Acta Materialia*, vol. 58, no. 11, pp. 3927–3938, 2010.

[25] S. R. MacEwen, C. E. Coleman, C. E. Ells, and J. Faber, "Dilation of h.c.p. zirconium by interstitial deuterium," *Acta Metallurgica*, vol. 33, no. 5, pp. 753–757, 1985.

[26] R. Nazarov, J. S. Majevadia, M. Patel, M. R. Wenman, D. S. Balint, J. Neugebauer, and A. P. Sutton, "First-principles calculation of the elastic dipole tensor of a point defect : Application to hydrogen in $\alpha$ -zirconium," *Physical review B*, vol. 241112, pp. 1–5, 2016.

[27] S. Q. Shi and Z. Xiao, "A quantitative phase field model for hydride precipitation in zirconium alloys: Part I. Development of quantitative free energy functional," *Journal of Nuclear Materials*, vol. 459, pp. 323–329, 2015.

[28] X. Q. Ma, S. Q. Shi, C. H. Woo, and L. Q. Chen, "Effect of applied load on nucleation and growth of $\gamma$-hydrides in zirconium," *Computational Materials Science*, vol. 23, no. 1-4, pp. 283–290, 2002.

[29] X. Q. Ma, S. Q. Shi, C. H. Woo, and L. Q. Chen, "The phase field model for hydrogen diffusion and $\gamma$-hydride precipitation in zirconium under non-uniformly applied stress," *Mechanics of Materials*, vol. 38, no. 1-2, pp. 3–10, 2006.

[30] Z. Xiao, M. Hao, X. Guo, G. Tang, and S. Q. Shi, "A quantitative phase field model for hydride precipitation in zirconium alloys: Part II. Modeling of temperature dependent hydride precipitation," *Journal of Nuclear Materials*, vol. 459, pp. 330–338, 2015.

[31] J. Bair, M. A. Zaeem, and M. Tonks, "A phase-field model to study the effects of temperature change on shape evolution of $\gamma$-hydrides in zirconium," *Journal of Physics D: Applied Physics*, vol. 49, no. 40, 2016.

[32] T. W. Heo, K. B. Colas, A. T. Motta, and L.-Q. Chen, "A phase-field model for hydride formation in polycrystalline metals : Application to $\delta$ -hydride in zirconium alloys," *Acta Materialia*, vol. 181, pp. 262–277, 2019.

[33] M. P. Puls, "Review of the thermodynamic basis for models of delayed hydride cracking rate in zirconium alloys," *Journal of Nuclear Materials*, vol. 393, no. 2, pp. 350–367, 2009.

[34] G. Simmons and H. Wang, *Single crystal elastic constants and calculated aggregate properties: a handbook*. Cambridge, Mass., M.I.T. Press, 1971.

[35] P. Burr, *Ab-initio modelling of Zr and Be alloys for nuclear applications*. PhD thesis, Imperial College London, 2015.

[36] J. Eshelby, "The determination of the elastic field of an ellipsoidal inclusion, and related problems," *Proceedings of the Royal Society of London A: Mathematical, Physical and Engineering Sciences*, vol. 241, no. 1226, pp. 376–396, 1957.

[37] P. Chemelle, D. B. Knorr, J. B. Van Der Sande, and R. M. Pelloux, "Morphology and composition of second phase particles in Zircaloy-2," *Journal of Nuclear Materials*, vol. 113, no. 1, pp. 58–64, 1983.

[38] J. P. Gros and J. F. Wadier, "Precipitate growth kinetics in Zircaloy-4," *Journal of Nuclear Materials*, vol. 172, no. 1, pp. 85–96, 1990.

[39] S. El Chamaa, M. Patel, C. M. Davies, and M. R. Wenman, "The Effect of Grain Boundaries and Second-Phase Particles on Hydride Precipitation in Zirconium Alloys," *MRS Advances*, vol. 3, no. 31, pp. 1749–1754, 2018.

[40] P. Zhang, M. Karimpour, D. Balint, J. Lin, and D. Farrugia, "A controlled Poisson Voronoi tessellation for grain and cohesive boundary generation applied to crystal plasticity analysis," *Computational Materials Science*, vol. 64, pp. 84–89, 2012.

[41] P. Lazzarin and R. Tovo, "A unified approach to the evaluation of linear elastic stress fields in the neighborhood of cracks and notches," *International Journal of Fracture*, vol. 78, no. 1, pp. 3–19, 1996.

[42] D. Nowell, D. Dini, and P. Duo, "Stress analysis of V-notches with and without cracks, with application to foreign object damage," *The Journal of Strain Analysis for Engineering Design*, vol. 38, no. 5, pp. 429–441, 2003.

[43] J. Willis, "Stress fields produced by dislocations in anisotropic media," *Philosophical Magazine*, vol. 21, no. 173, pp. 931–949, 1970.

[44] C. D. Cann, M. P. Puls, E. E. Sexton, and W. G. Hutchings, "The effect of metallurgical factors on hydride phases in zirconium," *Journal of Nuclear Materials*, vol. 126, no. 3, pp. 197–205, 1984.

[45] M. Patel, S. Waheed, M. R. Wenman, A. P. Sutton, and D. S. Balint, "Discrete dislocation plasticity modeling of hydrides in zirconium under thermal cycling," *MRS Advances*, vol. 2, no. 55, pp. 3353–3358, 2017.

[46] J. Cui, G. K. Shek, D. A. Scarth, and Z. Wang, "Delayed Hydride Cracking Initiation at Notches in Zr-2.5Nb Alloys," *Journal of Pressure Vessel Technology*, vol. 131, no. 4, p. 041407, 2009.

[47] Y. Guo, T. B. Britton, and A. J. Wilkinson, "Slip band-grain boundary interactions in commercial-purity titanium," vol. 76, pp. 1–12, 2014.

[48] H. Abdolvand, "Progressive modelling and experimentation of hydrogen diffusion and precipitation in anisotropic polycrystals," *International Journal of Plasticity*, vol. 116, pp. 39–61, 2019.

[49] S. M. Hanlon, S. Persaud, F. Long, and M. Daymond, "Advanced Characterization of Hydrides in Zirconium Alloys," *Proceedings of the 18th International Conference on Environmental Degradation of Materials in Nuclear Power Systems - Water Reactors*, 2018.

[50] G. J. C. Carpenter, "An in-situ study of the dissolution of $\gamma$-zirconium hydride in zirconium," *Journal of Nuclear Materials*, vol. 73, no. 2, pp. 190–197, 1978.